Spectral dependency of optical backscattering by marine particles from satellite remote sensing of the global ocean

Hubert Loisel, Jean-Marc Nicolas, Antoine Sciandra, Dariusz Stramski, Antoine Poteau

Spectral dependency of optical backscattering by marine particles from satellite remote sensing of the global ocean

Hubert Loisel,[1] Jean-Marc Nicolas,[2] Antoine Sciandra,[3] Dariusz Stramski,[4] and Antoine Poteau[1]

Received 27 October 2005; revised 20 April 2006; accepted 15 May 2006; published 20 September 2006.

[1] Knowledge of the relative proportion between small-sized and larger particles in the surface ocean is essential to understand the ocean ecology and biogeochemistry, including particle dynamics and carbon cycling. We show that this information may be assessed qualitatively from satellite observations of ocean color. Such capability is based on the estimation of spectral dependence, γ, of particulate backscattering coefficient, b_{bp}, which is sensitive to particle size distribution. Our results obtained from satellite observations of the global ocean are supported by in situ measurements, and they demonstrate a general decrease of the spectral slope γ from oligotrophic to eutrophic regimes, although significant regional differences are observed in the relationship between γ and the chlorophyll *a* concentration, Chl. To first approximation, such a decrease in γ is expected to be accompanied by an increased role of larger particles. This is consistent with our field data that show relatively high concentrations of submicron particles in very clear oceanic waters. Different seasonal patterns are also observed depending on the oceanic regions. The seasonal amplitude of γ is generally higher than that of Chl and b_{bp} in equatorial and tropical regions, and it is much lower at temperate latitudes. These spatio-temporal patterns are interpreted in terms of processes that modify the composition of particulate assemblages and physiology of phytoplankton in response to environmental forcing. The changes in γ are clearly related to variations in the mixed layer depth and photosynthetic available radiation.

Citation: Loisel, H., J.-M. Nicolas, A. Sciandra, D. Stramski, and A. Poteau (2006), Spectral dependency of optical backscattering by marine particles from satellite remote sensing of the global ocean, *J. Geophys. Res.*, *111*, C09024, doi:10.1029/2005JC003367.

1. Introduction

[2] In open ocean waters, suspended particulate matter is mostly composed of phytoplankton, heterotrophic organisms, viruses, and organic detritus of various sizes. Mineral particles are also present but their significance is usually limited to coastal areas. Particles scatter natural light back out of the ocean and into space, which can be detected by satellite ocean color sensors. The thickness of surface oceanic layer that is remotely sensed in the visible part of the spectrum typically varies from a few meters to about 60 meters, depending on the presence of optically significant constituents in water and light wavelength being used in the measurement [*Smith*, 1981]. Among the different particulate components, small-sized, mostly non-living, particles are believed to be generally a dominant source of the particulate backscattering coefficient in surface waters of the open ocean under conditions of no phytoplankton bloom [*Morel and Ahn*, 1991; *Stramski and Kiefer*, 1991; *Dupouy et al.*, 2003]. However, other scenarios associated with large variability in particulate assemblages in the global ocean are possible [*Stramski et al.*, 2004; *Stramski and Wozniak*, 2005]. For example, phytoplankton populations may have a higher contribution to b_{bp} than suggested by calculations for homogeneous spherical cells [*Kitchen and Zaneveld*, 1992].

[3] Processes of physical transport and biochemical interactions involving seawater constituents that are important to many areas of ocean science are affected by size of suspended particles in the ocean [*Lal*, 1977; *Koike et al.*, 1990]. For instance, large phytoplankton like diatoms or particulate aggregates composed of detritus, fecal pellets, and/or attached microorganisms are directly involved in carbon fluxes toward the interior of the ocean and subsequent sequestration of carbon in the deep ocean [*Treguer et al.*, 1995]. In contrast, small-sized particles (less than about 2 μm) that are numerically dominated by colloidal matter from the submicrometer range, such as non-living detrital particles, picophytoplankton, heterotrophic bacteria, and viruses do not have appreciable settling rates. Thus, these particles are mostly involved in regeneration processes in surface waters [*Falkowski et al.*, 1998]. The small-sized particles can, however, make a major contribution to the pool of particulate organic carbon (POC) in the surface

[1] ELICO - Université du Littoral - Côte d'Opale, Wimereux, France.
[2] Laboratoire d'Optique Atmosphérique, Lille, France.
[3] Laboratoire d'Océanologie de Villefranche-sur-Mer, Villefranche-sur-Mer, France.
[4] Scripps Institution of Oceanography, University of California, San Diego, California, USA.

0148-0227/06/2005JC003367

ocean [*Koike et al.*, 1990; *Longhurst et al.*, 1992]. Knowledge of the particle size distribution (PSD) is therefore of fundamental importance to ocean biogeochemistry and ecology.

[4] Recent marine ecosystem models attempt to include explicitly different sizes of marine particles to understand the ocean component of the global carbon cycle [*Aumont et al.*, 2003]. However, little is known about the temporal and large-scale spatial variability of PSD in the world's oceans. Only limited information is available locally from areas visited by oceanographic cruises during relatively short periods of time [*Bader*, 1970; *Sheldon et al.*, 1972; *Jonasz*, 1983; *Twardowski et al.*, 2001]. Here we show that relative proportion between small-sized and larger particles in the surface ocean can be, to first approximation, estimated from satellite remote sensing of ocean color, which offers a synoptic coverage of the global ocean. This capability is based on the estimation of spectral dependence of particulate backscattering coefficient, $b_{bp}(\lambda)$, which in turn depends on PSD.

[5] The spectral dependence of light scattering has been theoretically shown to be sensitive to the shape of PSD [*Morel*, 1976] and recent field studies indicated a trend of an increase in the spectral slope of backscattering γ with an increase in relative contribution of small-sized particles to the total particle concentration [*Reynolds et al.*, 2001]. Based on Mie scattering calculations, *Wozniak and Stramski* [2004] reported a remarkable increase in the γ slope with an increase in the PSD slope, ξ, for particles with high refractive index, which can be representative of minerogenic particles. For example, they showed that γ increases from 0.09 to 1.62 when ξ changes from -3.2 to -4.8 for relatively weakly absorbing mineral particles (these values are calculated from their Figure 4b). Similar trend will also hold for low refractive (organic) particles because γ is relatively insensitive to the refractive index [*Stramski et al.*, 2001]. The same calculations also indicated that γ is quite insensitive to particles with diameter D greater than 10 μm [*Wozniak and Stramski*, 2004]. For example, a decrease of the PSD upper cutoff from D = 500 μm to 10 μm produces almost no change in γ (as was shown for the case of $\xi = -4$). One may expect that similar trend will also hold for organic particles because the relative importance of small sized particles to backscattering increases as the refractive index decreases [*Stramski and Kiefer*, 1991]. Therefore, to first approximation, the variation in γ may be considered as an index of the variation in the relative proportion of small-sized and larger particles within the range from submicrometer particle sizes to a size of about 10 μm or even somewhat less. Generally, the higher γ is, the higher the proportion of small-sized particles within that size range is expected. We recall, however, that other scenarios of the relative roles of different particle sizes in backscattering cannot be excluded because of large variability in particulate assemblages in the global ocean [*Stramski et al.*, 2004]. For example, it is reasonable to expect that the backscattering slope γ can be affected by particles larger than 10 μm under conditions when large phytoplankton cells form blooms.

[6] We also note that the presence of air bubbles in oceanic surface layer may represent a significant source of light backscattering with consequences to ocean reflectance [*Terrill et al.*, 2001; *Stramski and Tegowski*, 2001; *Zhang et al.*, 2002]. Although much of the effect of bubble clouds may be removed through the foam and whitecap correction algorithm applied to processing of satellite ocean color data, some effect may still remain. At present, the lack of adequate information on the presence and properties of bubble clouds does not allow us to estimate these effects for the examined satellite images of ocean color and the derived spectral dependence of backscattering.

[7] In this study we apply an inverse optical model to satellite measurements of ocean color made with the Seaviewing Wide Field-of-view Sensor (SeaWiFS) to reveal the spatial and temporal variability in the spectral slope, γ of the $b_{bp}(\lambda)$ spectrum in the global ocean. The patterns of γ are compared to those of the chlorophyll *a* concentration and the particulate backscattering coefficient in oceanic regions characterized by different physical forcing and biogeochemical conditions.

2. Data and Methods

[8] The normalized water leaving radiances, $L_{wn}(\lambda)$, obtained from the fourth reprocessing of the SeaWiFS data, are used to derive the different bio-optical data products used in this study: Chl, $b_{bp}(\lambda)$, and γ. The $L_{wn}(\lambda)$ data were acquired from the NASA Goddard Distributed Active Archive Center and extracted using the SeaDAS software provided by NASA. Monthly Level 3 standard mapped images of $L_{wn}(\lambda)$ with a nominal 9 km $\times$ 9 km resolution collected from January 1998 to December 2002 over the global ocean are examined in this study. The chlorophyll *a* concentration, Chl, was derived from $L_{wn}(\lambda)$ according to the OC4v4 algorithm [*O'Reilly et al.*, 2000].

[9] Estimation of $b_{bp}(\lambda)$ and γ from satellite data of $L_{wn}(\lambda)$ is carried out as follows. First, the particulate backscattering coefficient, $b_{bp}(\lambda)$, is estimated from SeaWiFS-derived $L_{wn}(\lambda)$ at three wavelengths λ = 490, 510, and 555 nm. This derivation is based on an inverse model [*Loisel and Stramski*, 2000], which allows to retrieve the absorption and backscattering coefficients from $L_{wn}(\lambda)$. This model was tested against in situ measurements performed in both near-shore and off-shore waters [*Loisel et al.*, 2001, 2002; *Melin et al.*, 2005]. An important attribute of this model is that it is independent of the spectral behavior of the absorption and backscattering coefficients of seawater. This model requires the irradiance reflectance just beneath the sea surface, $R(0^-, \lambda)$, the average attenuation coefficient for downwelling irradiance, $K_d(\lambda)$, between the surface and the first attenuation depth, and the solar zenith angle as input parameters. The required values of $K_d(\lambda)$ and $R(0^-, \lambda)$ were calculated from SeaWiFS-derived $L_{wn}(\lambda)$ according to the procedure described in *Loisel et al.* [2001]. This procedure uses empirical relationships between $K_d(\lambda)$ and $L_{wn}(\lambda)$. At 490 nm, $K_d(490)$ is derived from the algorithm proposed by Mueller (2000), which uses the ratio of L_{wn} at 490 and 555 nm. Two simple linear relationships are then used to derive $K_d(510)$ and $K_d(555)$ from $K_d(490)$:

$$K_d(510) = 0.839\, K_d(490) + 0.0184 \quad (1)$$

$$K_d(555) = 0.611\, K_d(490) + 0.056 \quad (2)$$

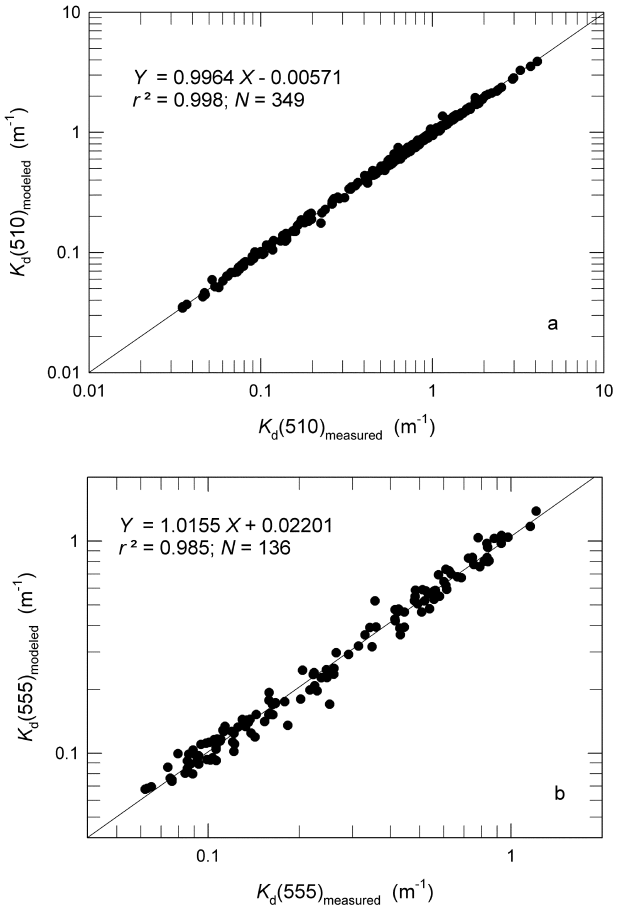

Figure 1. Comparison of the modeled and the measured vertical attenuation coefficient of downwelling irradiance at (a) 510 nm, and (b) 555 nm. The measured $K_d(\lambda)$ values are from the NOMAD data set [*Werdell and Bailey*, 2005], whereas the modeled $K_d(\lambda)$ values are calculated from equations (1) and (2) using the measured $K_d(490)$ values as input parameter. Solid lines represent the least squares linear fits. The regression equations, the determination coefficient (r^2), and the number of observations (N) are also shown.

These two relationships were developed from in situ measurements acquired in oceanic waters around Europe [*Loisel et al.*, 2001]. The performance of these two empirical equations are evaluated against independent data collected in surface waters of other oceanic regions [*Werdell and Bailey*, 2005]. Figure 1 shows that there is a very good agreement between the modeled and the measured values for $K_d(510)$ (the determination coefficient $r^2 = 0.998$) and for $K_d(555)$ ($r^2 = 0.984$). The absolute average relative differences ($= 100 \frac{1}{N} \sum_{1}^{N} \left| \frac{K_d(\lambda)_{modeled} - K_d(\lambda)_{measured}}{(K_d(\lambda)_{modeled} + K_d(\lambda)_{measured})/2} \right|$) between the modeled and measured $K_d(\lambda)$ values at 510 and 555 nm are 3.5 % and 8.9 %, respectively.

[10] Having obtained the three spectral values of $b_{bp}(\lambda)$ at 490, 510, and 555 nm from the *Loisel and Stramski* [2000] inverse model, the next step of our approach is the estimation of γ from these values of $b_{bp}(\lambda)$. Field studies showed that the spectral shape of $b_{bp}(\lambda)$ can be approximated by a power law $b_{bp}(\lambda) \sim \lambda^{-\gamma}$ [*Reynolds et al.*, 2001; *Stramska et al.*, 2003]. The use of this common spectral model will allow comparison with γ values estimated in previous studies [*Sathyendranath et al.*, 1989; *Hoge and Lyon*, 1996; *Carder et al.*, 1999; *Ciotti et al.*, 1999; *Toole and Siegel*, 2001; *Cota et al.*, 2003]. We calculated γ by linear regression between log $[b_{bp}(\lambda)]$ and log λ, where γ is the slope of the regression. The determination coefficients of the least squares fits between log $[b_{bp}(\lambda)]$ and log λ performed over each 9x9 pixel of the monthly data products of $b_{bp}(\lambda)$ range between 0.95 and 0.99 for the global ocean (the lowest r^2 values are found at high latitudes).

[11] The spectral slope γ of $b_{bp}(\lambda)$ varies rather weakly in the ocean, typically from 0 to 3. Therefore, it appears to be especially important to evaluate potential uncertainties in the estimation of γ from satellite observations. In addition to uncertainties related to the atmospheric correction (i.e., the estimation of water leaving radiances from the SeaWiFS signal measured at the top of the atmosphere), three other major sources of uncertainties can be identified in the γ estimation from our algorithm: first, the sensitivity of the *Loisel and Stramski* [2000] model to the ratio of molecular scattering to total scattering (i.e., the η parameter), second, uncertainties associated with the estimation of $K_d(\lambda)$ from $L_{wn}(\lambda)$, and finally, the assumption of a power function spectral model for $b_{bp}(\lambda)$. The discussion of the impact of inaccurate atmospheric correction on the retrieval of γ is beyond the scope of this paper. We simply assume that the $L_{wn}(\lambda)$ values are retrieved with adequate accuracy from SeaWiFS measurements. Recent validation studies show relatively good results for the satellite-derived $L_{wn}(\lambda)$ in the green part of the spectrum. The median absolute percent differences between in situ–derived L_{wn} and satellite-derived L_{wn} at 490, 510 and 555 nm are 15.1%, 13.7, and 16.9 %, respectively (http://seabass.gsfc.nasa.gov/matchup_results.html). Moreover, the absolute values of $L_{wn}(\lambda)$ are not particularly critical to our study because our estimation of γ depends mainly on the relative value of $L_{wn}(\lambda)$ at 490 nm compared to that at 555 nm, which reduces the impact of imperfect atmospheric correction.

[12] Our inverse model is weakly dependent on the parameter η, which is defined as the ratio of molecular scattering to total scattering (see equations (18) and (19) in *Loisel and Stramski* [2000]). This dependence has a significant effect on the retrieval of b_{bp} only for large solar zenith angles and high backscattering values [*Loisel and Stramski*, 2000]. Because of large uncertainty in the estimation of η from space [*Loisel et al.*, 2001], η was here kept constant. Based on in situ measurements performed in coastal and open ocean waters, the η value was assumed to be 0.03 (see Figure 6b in *Loisel et al.* [2001]). A sensitivity analysis performed on a data set generated with radiative transfer calculations for various inherent optical properties of water, shows that the absolute average relative difference between the γ values estimated by our model using the true η values as inputs, and those estimated with $\eta = 0.03$ is only 2.67%. A complete description of the synthetic data set used in these sensitivity tests is available on the International Ocean Color Coordinating Group web site (http://www.ioccg.org/groups/OCAG_data.html). Note also that the sensitivity of

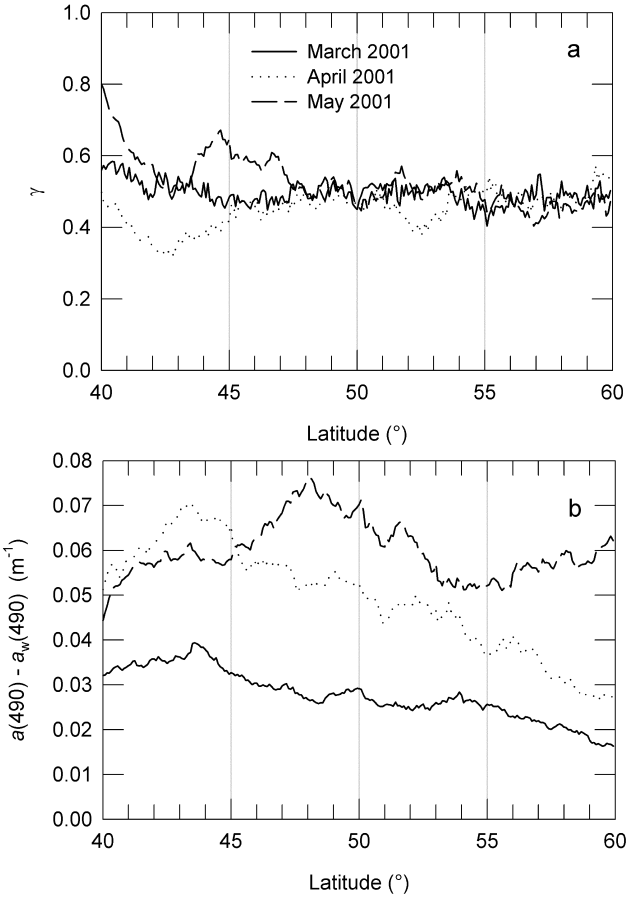

Figure 2. Mean values of (a) γ and (b) $a(490) - a_w(490)$ calculated for the [40°–60°N] latitudinal zone in March (solid lines), April (dotted lines), and May (dashed lines) of the year 2001.

the model retrieval is not affected by changes in the shape of the particle scattering phase function, at least for the tested values of backscattering ratio ranging from 0.0054 to 0.034 [*Loisel and Stramski*, 2000]. This range of variability is consistent with recent in situ measurements performed in different environments [*Twardowski et al.*, 2001; *Boss et al.*, 2004].

[13] The next potential source of uncertainty is related to the estimation of $K_d(\lambda)$ from space. To investigate the effect of error in $K_d(\lambda)$ on the γ retrieval, a sensitivity analysis was performed with the synthetic IOCCG data set. This analysis shows that the resulting error in γ is roughly proportional to the error in $K_d(\lambda)$. For example, uncertainties of 10% and 30% in $K_d(490)$ that is used to estimate $K_d(510)$ and $K_d(555)$, lead to uncertainties of 4.6% and 9.3% in γ, respectively. Therefore, when large errors in $K_d(\lambda)$ are suspected, typically in coastal areas, the retrieved γ values should be interpreted with particular caution.

[14] Finally, the last source of uncertainty in the estimation of γ is related to the assumption of spectral behavior of $b_{bp}(\lambda)$. The potential problem is related to the presence of strongly absorbing matter in water because the spectral shape of $b_{bp}(\lambda)$ can differ from a monotonic power function, especially within the strong absorption bands of phytoplankton where backscattering is reduced [*Bricaud et al.*, 1983]. We use the three wavelengths that are away from the main absorption bands of phytoplankton near 440 nm and 670 nm. Therefore, the potential effects of absorption on the estimation of the general spectral slope of backscattering are minimized. However, some absorption, especially at 490 nm, may still affect our retrieval of γ. To evaluate this effect, we compare the spatio-temporal patterns of γ with those of the absorption coefficient at 490 nm, $a(490)$, both being retrieved from $L_{wn}(\lambda)$ using the *Loisel and Stramski* [2000] model.

[15] This sensitivity analysis was performed for the northern Atlantic during the phytoplankton bloom period when the effect of the absorption on the γ retrieval should be obvious. Figure 2 illustrates the monthly zonal mean of the non-water absorption, $a(490) - a_w(490)$ (where the subscript w indicates pure water contribution), and the spectral slope, γ, in the northern Atlantic from March through May 2001. These results were derived from the Level-3 monthly binned SeaWiFS data of $L_{wn}(\lambda)$. If the γ retrieval is affected by absorption, high absorption will reduce γ, and vice versa. While such behavior can be observed for the March-April period between 40°N and 45°N, other features in Figure 2 suggest that our retrieval of γ is weakly dependent or nearly independent on the absorption coefficient. For example, whereas $a(490) - a_w(490)$ decreases from 45°N to 60°N by a factor of 2.0 and 2.4 in March and April, respectively, γ remains fairly constant (the same observation holds in May). Also, while $a(490) - a_w(490)$ increases significantly from March through May at latitudes >45°N, γ exhibits very little changes.

[16] Field measurements of particle size distribution (PSD) were performed on water samples collected during the Biogeochemistry and Optics South Pacific Experiment (BIOSOPE) in October–November 2004. The PSD measurements in the submicrometer range have been seldom made but steep slopes in the submicrometer range were observed previously in clear waters near Bahama Islands [*Brown and Gordon*, 1974] and in the northwest Pacific coastal environments [*Yamasaki et al.*, 1998]. Because accurate counting and sizing of very small particles is generally difficult, some comments on our measurement methods in the south Pacific are in order. These measurements were made at sea on board the ship immediately after collection of water samples with a CTD/rosette cast. The Multisizer 3 Coulter Counter (Beckman Coulter, Inc.) was set up in a laboratory in a way that ship vibrations were efficiently reduced. The background "noise" (i.e., the instrument counts) was very low and was routinely checked by measurements on clear seawater filtered multiple times through a 0.2-μm filter. The background counts with filtered seawater were always less than 5% of the sample counts, with a mean value of 2.7%. This low level of background counts allowed us to analyze data down to a particle size of 0.6 μm when we used a 30-μm aperture tube. Occasionally we used a 20-μm aperture tube that provided reliable measurements for particles as small as about 0.5 μm. Importantly, the results obtained with 30-μm and 20-μm aperture tubes for the same sample were consistent within the overlapping size range. The PSD data were obtained typically with a 30-μm aperture tube using 300 size bins

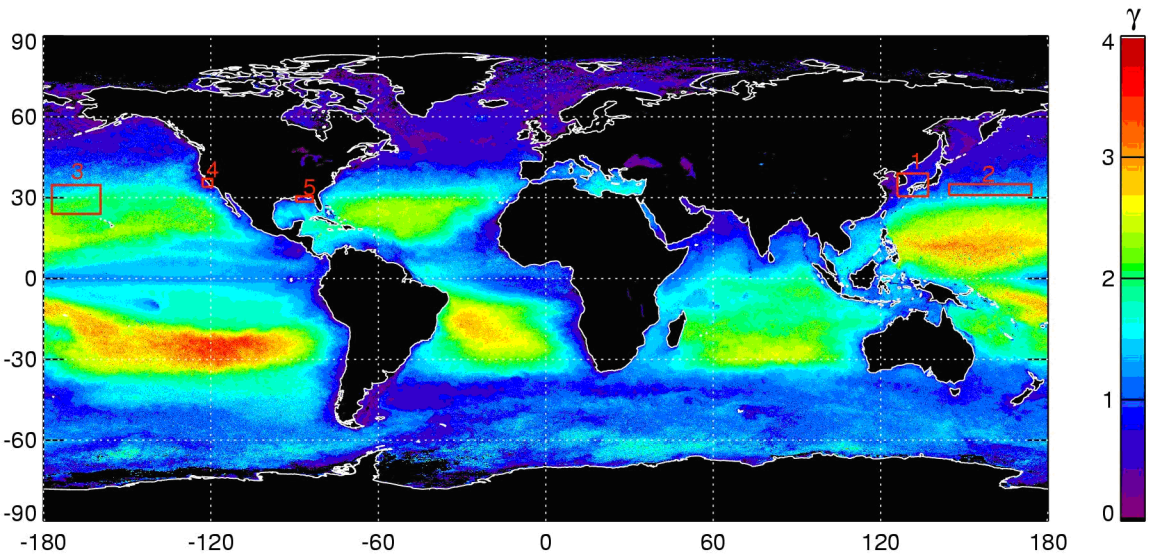

Figure 3. Global map of annual mean value of γ in 2001 derived from SeaWiFS imagery. The red frames identified by the numbers 1 to 5 show specific regions where in situ data of γ were collected in 2001. These data were extracted from the SeaBASS archive. For each data set the mean and standard deviation values of γ are as follows; region 1: 1.94 ± 0.5; region 2: 2.8 ± 0.36; region 3: 2.01 ± 0.55; region 4: 1.06 ± 0.42; and region 5: 1.17 ± 0.68. Only two coincident satellite-derived and field data of γ are available from these regions. The satellite to in situ ratio of γ for these two matchup data points are 0.35 and 0.90.

between 0.6 and 18 μm. The final PSD for a given sample was calculated by averaging results from 8 (sometimes a few more) replicate measurements, each of which was made on 0.5 mL of the sample.

3. Results

[17] Our algorithm was applied to determine the distribution of γ in the global ocean from the Level-3 monthly binned $L_{wn}(\lambda)$ data collected by the SeaWiFS sensor from 1998 to 2002. The results presented are based primarily on data from the year 2001 which is not influenced by the El Niño/La Niña events that affect the tropical Pacific every 2 to 7 years. We note, however, that the main spatio-temporal patterns reported here, as well as the relationships between γ, $b_{bp}(\lambda)$ and Chl, do not change drastically from one year to another. For comparison, some results from satellite data collected in 1998, when a strong El Niño/La Niña episode occurred, are also provided.

[18] The monthly mean γ values of the year 2001 were averaged to obtain the global distribution of yearly γ (Figure 3). Figure 4 shows a histogram of γ for 2001 obtained from data presented in Figure 3. The mean value of γ for the global ocean is 1.37 (with a standard deviation ±0.42). The overall range of variability in γ is in good agreement with predictions from earlier studies [*Sathyendranath et al.*, 1989; *Hoge and Lyon*, 1996; *Carder et al.*, 1999; *Ciotti et al.*, 1999; *Reynolds et al.*, 2001; *Toole and Siegel*, 2001; *Stramska et al.*, 2003; *Cota et al.*, 2003] that showed that the wavelength dependence of b_{bp} ranges from λ^{-3} to λ^{0} (see also caption of Figure 3). According to our study, the values of γ higher than 2.5 are relatively uncommon and represent only 6.1% of the ocean surface in 2001. High γ values are observed in subtropical gyres where large scale downwelling is expected, and where primary production is mostly sustained by regeneration processes involving picoplankton [*Falkowski et al.*, 1998]. The maximum γ of 3.5 is observed in the center of the South Pacific gyre, where the surface chlorophyll concentration, Chl, is often as low as 0.02 mg m^{-3}. This maximum γ within the biologically poorest area of the ocean [*Claustre and Maritorena*, 2003] reinforces the idea of a system dominated by relatively high proportion of submicron particles, including non-living colloidal matter [*Dandonneau et al.*, 2003]. The lowest γ values in the range 0–0.5 in Figure 3 are found in coastal areas and at high and temperate latitudes. Compared to subtropical gyres, these areas are characterized by much higher surface Chl (up to a factor of ≈10) supported by net inputs of new nutrients injected from below the euphotic zone by advection or vertical mixing, and/or terrestrial sources.

[19] The highest values of γ in the South Pacific gyre are consistent with our field measurements of particle size distribution (PSD), which indicated a relatively large role of submicrometer particles in that region. The PSD measurements of surface water samples during the BIOSOPE cruise (see Figure 5a for the cruise track) showed that the slope of PSD is much steeper in the submicrometer range than for larger particles (Figures 5b and 5c). The results in Figure 5b indicate that a model of PSD with a single slope ξ over the entire size range examined can lead to significant underestimation of submicrometer particle concentration. For example, we estimated that the total particle volume in the 0.2–1 μm size range is lower by a factor of 10 if we apply a single slope of ξ = −3.3 obtained from a broad size spectrum that extends to particle size of 10 μm instead of the measured slope of −6.33 in the submicron range.

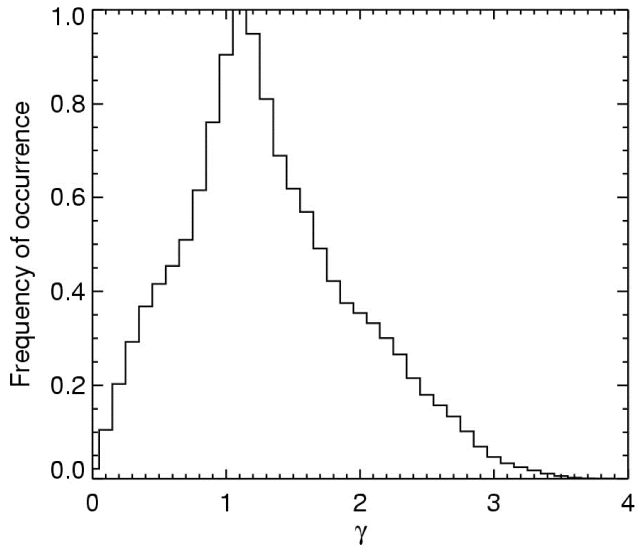

Figure 4. Histogram of the annual mean value of γ in 2001 derived from SeaWiFS for the global ocean.

[20] The global distributions of γ are compared for the months of January and July of 1998 and 2001 in Figure 6. In contrast to 2001, the year 1998 was greatly affected by the El Niño/La Niña events. The maximum sea level anomaly associated with El Niño occurred in boreal winter 1997/1998, and the La Niña event was well established in summer/fall 1998. Although the main spatial patterns in the yearly mean γ shown in Figure 3 are apparent in Figure 6, this figure also reveals the presence of seasonal variations. As a general statement, the γ values are much greater in summer than in winter, which holds for both the northern and southern hemisphere. In the northern hemisphere, the monthly mean γ increases from January (γ = 0.71 ± 1.9 in 1998 and 0.66 ± 2.0 in 2001) to July (γ = 1.35 ± 1.16 in 1998 and 1.29 ± 1.19 in 2001), on average, by a factor of 1.92 and 1.95 in 1998 and 2001 respectively. In the southern hemisphere, γ decreases from January (γ = 1.8 ± 0.86 in 1998 and 1.78 ± 0.87 in 2001) to July (γ = 0.61 ± 2.1 in 1998 and 0.715 ± 2.05 in 2001) by a factor of 2.95 and 2.5 in 1998 and 2001 respectively. These seasonal patterns suggest that the proportion of small-sized particles compared to larger particles generally increases from winter to summer in the surface oceanic waters. In the equatorial Pacific Ocean, the monthly mean γ values do not change significantly between January (1.51 ± 0.62) and July (1.51 ± 0.64) in 2001, but decrease by 11% between January (1.70 ± 0.63) and July (1.53 ± 0.65) in 1998. These values were calculated for the [10°S–10°N] latitudinal zone. The chlorophyll *a* concentrations in equatorial Pacific also exhibit similar mean values in January and July 2001, but increase by 14% between January and July 1998 (not shown here). These patterns are related to the weakening of the equatorial upwelling during El Niño and the strengthening of the upwelling during the transition to the La Niña conditions.

[21] For the global ocean, the monthly mean values of γ in the year 2001 decrease, on average, by a factor 1.4 between January (γ = 1.40 ± 1.46) and July (γ = 1.0 ± 1.7). In 1998, these changes are similar, that is γ = 1.42 (±1.39) in January and γ = 0.97 (±1.79) in July. We note that this general trend of variation in γ between the month of January and July over the global ocean is qualitatively similar to that observed in the southern hemisphere, but opposite to that observed in the northern hemisphere. This can be attributed to a larger surface area of the ocean in the southern hemisphere compared to the northern hemisphere. In addition, we see large variability in γ over the global ocean for both months and both years examined as the standard deviation values for the images shown in Figure 6 are similar to or larger than the mean values. The variability in γ is also illustrated by histograms shown in Figure 6. We find, for example, that the values of γ lower than 1.0 represent 25% and 43% of the ocean surface in January and July 2001, respectively. The values higher than 2.5 represent 13% of the ocean surface in January 2001 and 7% of the ocean surface in July 2001. These proportions are nearly the same for 1998.

[22] We note that the seasonal variability revealed by the mean γ values calculated over the global ocean between the months of January and July, as discussed above with regard to results presented in Figure 6, can be somewhat biased by the fact that different surface areas of the ocean in the northern and southern hemispheres are accessible to satellite observations during different seasons. For example, whereas the whole southern hemisphere is observed during the boreal winter (January), the large areas of the Southern Ocean at latitudes higher than approximately 50°S are not observed during the boreal summer (July). By restricting the ocean to the [50°S–50°N] latitudinal zone, the monthly mean values of γ in the year 2001 decrease, on average, by a factor 1.2 between January (γ = 1.49 ± 1.36) and July (γ = 1.24 ± 1.33). This change, which is attributed primarily to the Southern Ocean, is smaller by 14% than that calculated from data collected over the entire ocean. The values of γ lower than 1.0 represent 25% and 34% of the ocean surface in the [50°S–50°N] latitudinal zone in January and July 2001, respectively (as compared to 25% and 43% when the entire ocean is considered). For comparison, Figure 6 includes histograms of γ for both the entire global ocean and the ocean restricted to the [50°S–50°N] latitudinal zone.

[23] The spatial distribution of the monthly or annual mean values of γ is consistent with a prediction of a decrease of γ from oligotrophic (low Chl) to eutrophic (high Chl) regions [*Ciotti et al.*, 1999; *Morel and Maritorena*, 2001]. A linear regression model for satellite-derived data of monthly γ versus log(Chl) taken from the global ocean on a per pixel basis from the year 2001 yields a relationship with a slope of −1.45 (Figure 7a). The data points are, however, scattered considerably around the general trend line, especially at intermediate and high Chl values. A detailed analysis reveals significant regional differences in the γ vs. log(Chl) relationship. A tight relation is observed at tropical (10°–30°N) and temperate (30°–50°N) latitudes in the northern Atlantic ($r^2 > 0.8$ and slope ≈ −1.25 in both regions). The correlation breaks down in the equatorial region of the northern Atlantic ($r^2 = 0.45$ and slope = −0.55). In the northern Pacific, the γ vs. log(Chl) relationship is always significant in equatorial, tropical, and temperate regions ($r^2 > 0.76$) but the slope of the relationship

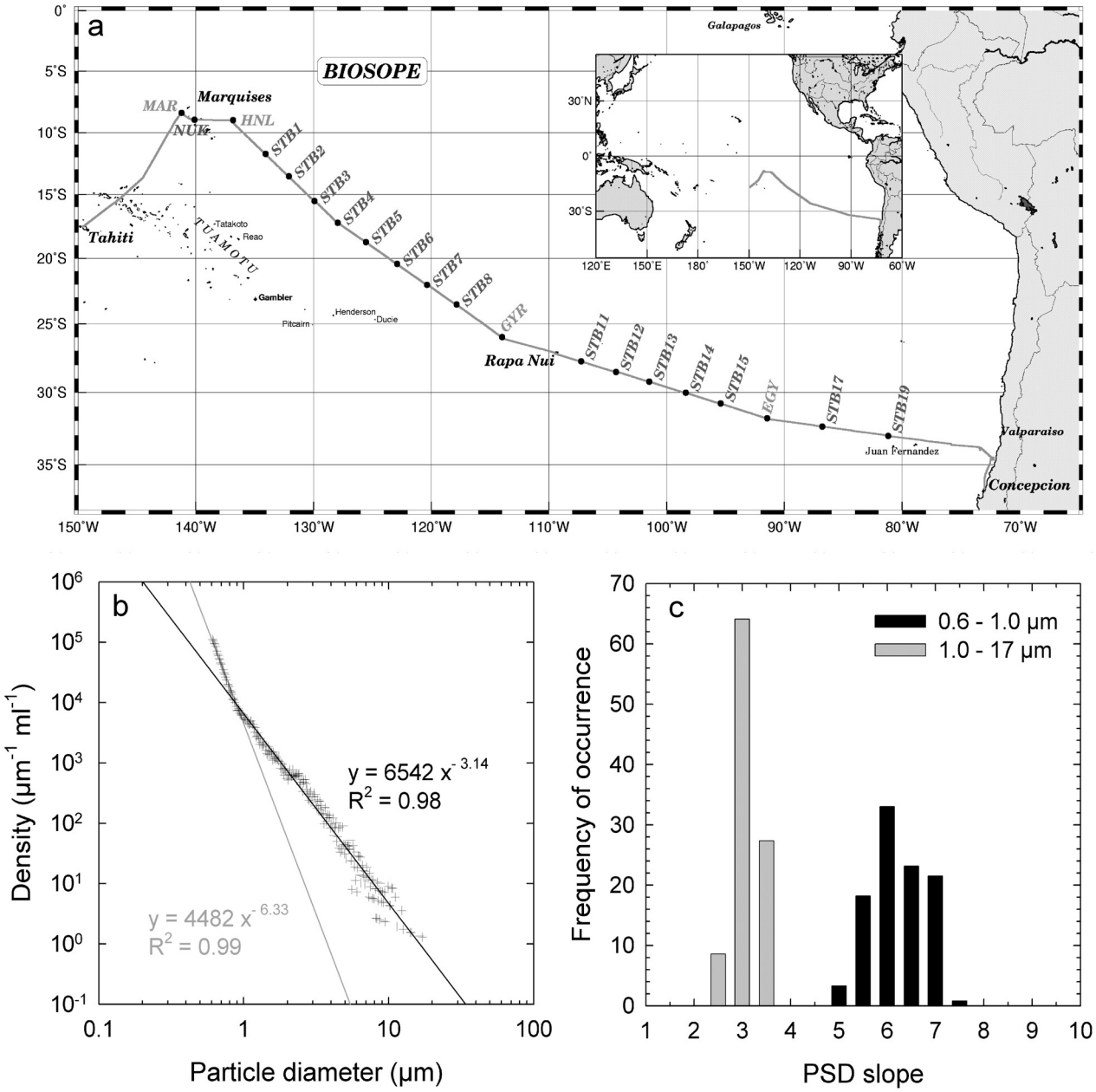

Figure 5. (a) Location of the stations visited during the Biogeochemistry and Optics South Pacific Experiment (BIOSOPE) conducted in the south tropical Pacific in November and December 2004. The STB stations correspond to short (6 hours) stations, whereas the EGY, GYR, HNL, and MAR stations correspond to long (3–6 days) stations. (b) The density function of particle size distribution measured with a Multisizer 3 for a sample collected in surface waters of the south Pacific gyre (26°S, 114°W) on 14 November 2004 during the BIOSOPE cruise. The grey and black lines correspond to power function fits for the 0.6–1.0 μm and 1.0–17 μm size ranges, respectively. The power function equations and the values of the determination coefficient are also shown. (c) Histograms of the PSD slope measured in the 0.6–1.0 μm and 1.0–17 μm size range on 109 surface water samples collected during the BIOSOPE cruise. The average values of the coefficient of variation for the PSD slopes calculated for the 0.6–1.0 μm and 1.0–17 μm size ranges are 2.96%, and 2.51%, respectively. The average values of the coefficient of determination for the log-transformed variables of particle concentration and particle diameter calculated for the 0.6–1.0 μm and 1.0–17 μm size ranges are 0.96, and 0.94, respectively. The PSD data presented here were collected mainly at the MAR, HNL, GYR, and EGY stations.

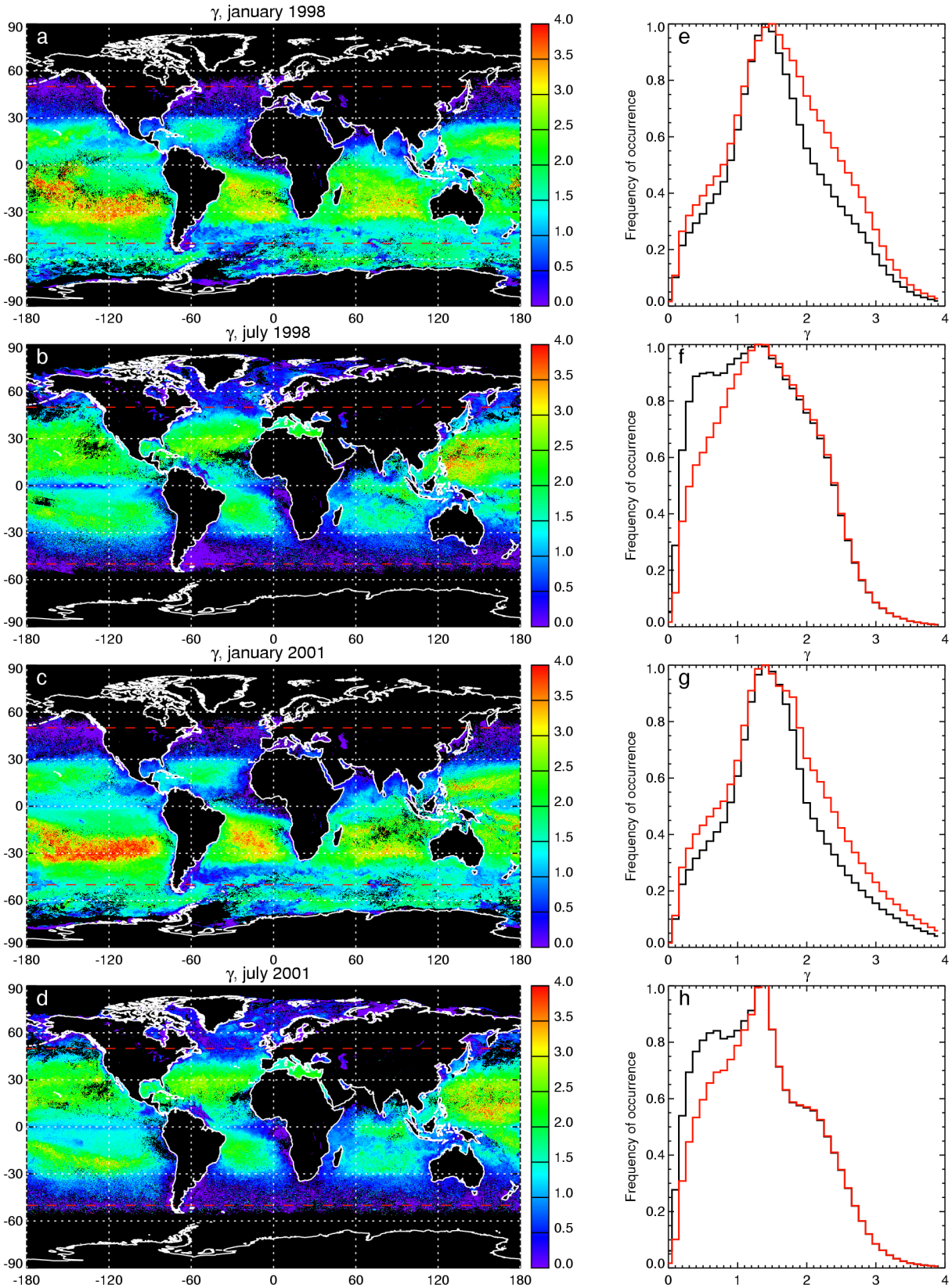

Figure 6. Global maps of monthly γ derived from SeaWiFS imagery for (a) January 1998, (b) July 1998, (c) January 2001, and (d) July 2001. Histograms of the monthly mean values of γ for (e) January 1998, (f) July 1998, (g) January 2001, and (h) July 2001. Histograms of γ for the entire global ocean are shown in black, whereas histograms in red represent the γ values for the ocean within the [50°S–50°N] latitudinal zone.

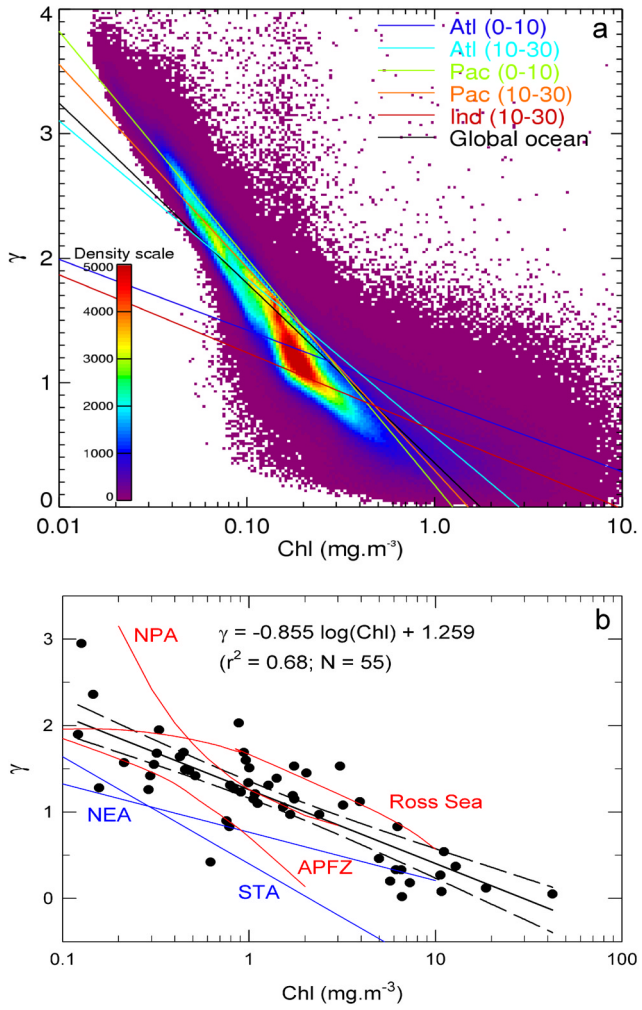

Figure 7. (a) Variation of γ as a function of chlorophyll *a* concentration, Chl, in the global ocean for monthly data from SeaWiFS observations in 2001. The colored lines represent the linear fit between γ and log(Chl) for different regions of the Atlantic (Atl), Pacific (Pac), and Indian (Ind) Oceans for the 0°–10°N and 10°–30°N latitudinal zones, as indicated. The black line is the fit for the global data set. (b) Solid circles show γ as a function of Chl from field measurements performed in 2001 in the various oceanic regions identified in Figure 1. Chl was determined using high performance liquid chromatography (HPLC) method, and γ was calculated from in situ b_{bp} measurements made with Hydroscat-6 (HobiLabs, Inc) instrument. The solid black line corresponds to the logarithmic function fit to these points, and the dashed line to the 95% confidence interval. The equation of the least squares fit, the r^2 coefficient, and the number of observations (N) are shown. For comparison, the relationships previously obtained from field measurements (red lines) in the Ross Sea [*Reynolds et al.*, 2001], the Antarctic Polar Front Zone, APFZ [*Reynolds et al.*, 2001], and in the north polar Atlantic, NPA [*Stramska et al.*, 2003], along with two examples of relationships obtained in this study from remote sensing (blue lines) in the North Atlantic, NEA, and the South Tropical Atlantic, STA, are shown.

decreases from the equatorial region (−1.8) to temperate latitudes (−1.18). In the equatorial region of the northern Indian Ocean, the behavior of γ with log(Chl) (r^2 = 0.75, slope = −0.95) differs from that observed in tropical latitudes (r^2 = 0.63, slope = −0.6). Such large spatial variability in the γ vs. log(Chl) relationship probably reflects differences in the composition of suspended particulate matter, including variations in the relative proportion of authotrophic, heterotrophic, and detrital particles, as well as changes in phytoplankton community structure. This general trend of a decrease in γ with Chl is supported by recent in situ measurements from various oceanic regions although the correlation for these field data is rather weak (Figure 7b). A similar trend is also observed between γ and b_{bp}(490) over the global ocean (not shown). The decrease in γ with b_{bp}(490) is also highly variable depending on the region, and the relationship between γ and log[b_{bp}(490)] shows generally more scatter in data points than γ vs. log(Chl).

[24] In addition to the regional differentiation of the γ vs. log(Chl) relationship, our results show that the patterns of temporal variation in γ throughout the year differ significantly from those of Chl and b_{bp}(490) within the global ocean. This is illustrated by global maps of the coefficient of variation for γ, Chl, and b_{bp}(490) (Figure 8), which were calculated using monthly composites of satellite-derived data from 2001. The spatial distribution of the coefficient of variation for γ may significantly differ from that of Chl and b_{bp}(490), and generally shows drastic differences in magnitude. The seasonal signals of γ, Chl, and b_{bp}(490) are more pronounced at higher than lower latitudes. As a general statement, the coefficient of variation of γ is generally lower than that of Chl and b_{bp}(490), and is also more evenly distributed in space. These differences indicate that the seasonal variations of γ are not only related to variations in Chl and b_{bp}(490), but seem also to be controlled partly by other sources of variability as discussed below.

[25] Time series of monthly data of Chl, b_{bp}(490), and γ show different patterns in oceanic regions that are characterized by different physical forcing and biogeochemical conditions. This is clearly seen for three major systems of the global ocean, the equatorial Pacific, the south tropical Pacific, and the north temperate Atlantic (Figure 9). In the southern equatorial zone of Pacific, where the photosynthetic available radiation, PAR, and mixed layer depth, MLD, values exhibit relatively weak monthly variations, the seasonal pattern of γ is generally reverse to that of Chl and b_{bp}(490) (Figures 9a and 9b). The parallel changes of Chl and b_{bp}(490) in this region indicate the covariation of phytoplankton pigment concentration and particulate pool that controls b_{bp}. The decrease of γ with an increase in the concentration of particulate pool and pigment concentration (for example, October through December) suggests the decreasing role of small-sized particles compared to larger particles during that period. This temporal pattern is consistent with a general trend of a decrease of γ from oligotrophic to eutrophic regions. In the south tropical Pacific, where the seasonal variations of PAR and MLD are more pronounced than in the equatorial zone, the seasonal patterns of Chl and b_{bp}(490) are opposite to one another (Figures 9c and 9d). This result can be caused by

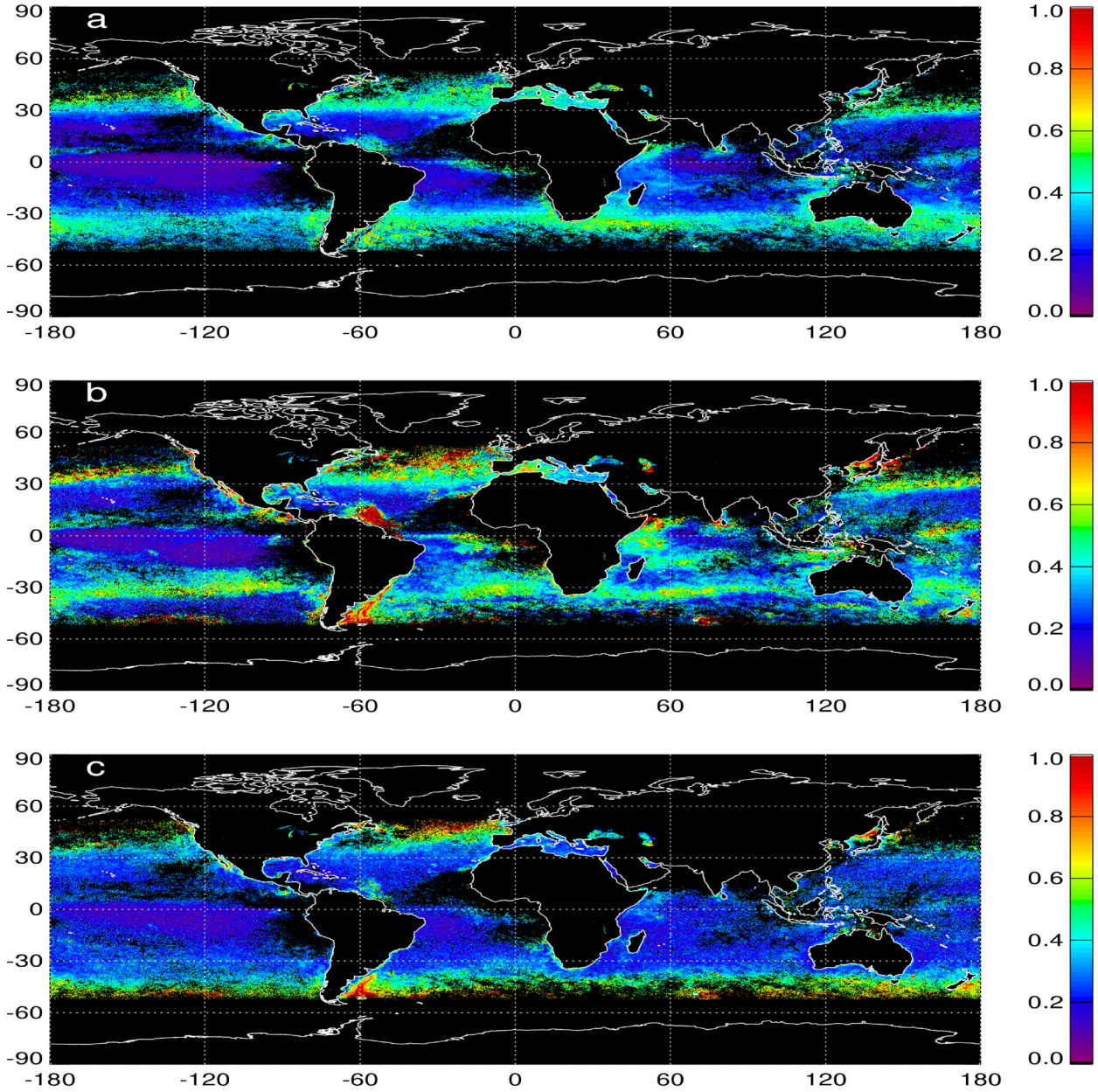

Figure 8. Coefficient of variation (i.e., a ratio of standard deviation to the annual mean) calculated from monthly data of (a) γ, (b) Chl, and (c) $b_{bp}(490)$ in the global ocean for the year 2001. Only pixels with 12 months of data are used to calculate the coefficient of variation.

the net accumulation of small, mainly non-living particles in the summer stratified layer [*Loisel et al.*, 2002]. This is supported by the parallel seasonal progression of γ and $b_{bp}(490)$, indicating that the increase of b_{bp} in summer is due primarily to increasing proportion of small particles. Another factor that can play a role in determining the seasonal patterns in Figures 9c and 9d is the variation in the chlorophyll-to-carbon (Chl/C) ratio in surface phytoplankton population undergoing photoacclimation [*Loisel et al.*, 2002; *Behrenfeld et al.*, 2005]. This is because the low Chl/C ratio during the austral summer in this region can indicate that relatively low bulk concentrations of Chl are accompanied by relatively high backscattering.

[26] At higher latitudes, where MLD is characterized by deep winter mixing and strong summer stratification, γ shows a different seasonal pattern compared to Chl and $b_{bp}(490)$ as illustrated for the north temperate Atlantic (Figures 9e and 9f). The maximum of γ is reached in summer (July), which is two months after the maximum of Chl and b_{bp} occurring in April. This pattern, also observed in the northern Pacific Ocean (not shown here), suggests that the dynamics of the particulate assemblage is closely related to the processes of growth and decline of phytoplankton population. From January to May, γ has a relatively small and constant value, whereas Chl increases by a factor of about 2, which is consistent with

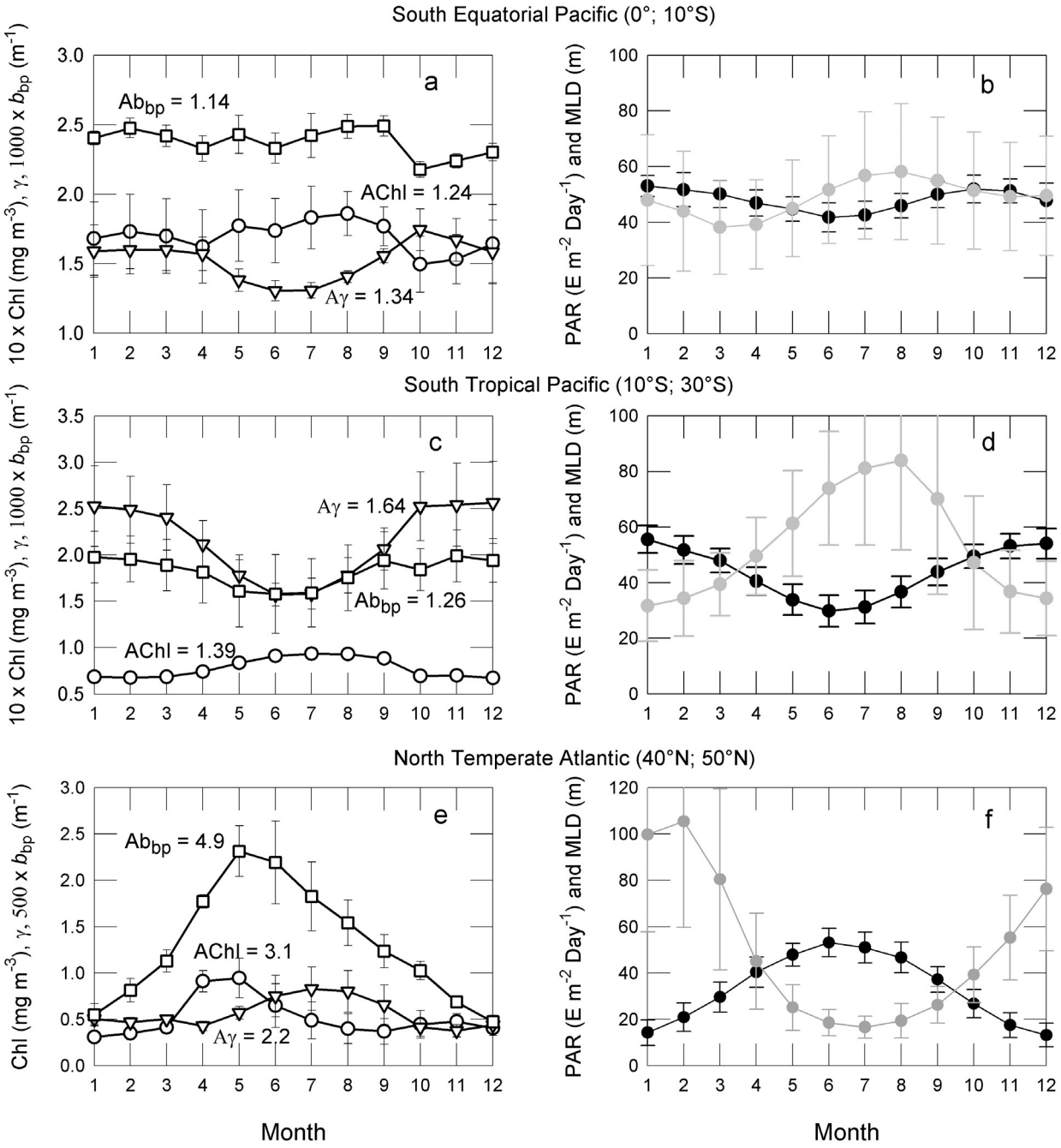

Figure 9. (left) Seasonal variations in monthly values of Chl (circle), $b_{bp}(490)$ (square), and γ (triangle) for different latitudinal zones as indicated. The data points correspond to monthly mean values and the vertical bars show the standard deviation for each month. The values of the seasonal amplitude for each parameter (AChl, Ab_{bp}, Aγ) calculated as the ratio of the maximum value of monthly means to the minimum value of monthly means are also shown on each panel. (right) For comparison, the environmental changes represented by monthly values of photosynthetically available radiation (PAR) and mixed layer depth (MLD) are shown. The PAR values are from SeaWiFS data [*Frouin et al.*, 2003], whereas MLD values are from a recent global climatology [*De Boyer Montégut et al.*, 2004] which was built from high vertical resolution in situ data collected from 1941 to 2002 in the world oceans.

the period of phytoplankton growth and net accumulation. The value of γ shows the largest change during the post-bloom period, when proportion between phytoplankton cells and small-sized nonliving particles changes due to phytoplankton decline and MLD variations. In contrast to the two other regions, the seasonal amplitude of γ at temperate latitudes is always lower that that of Chl and b_{bp}.

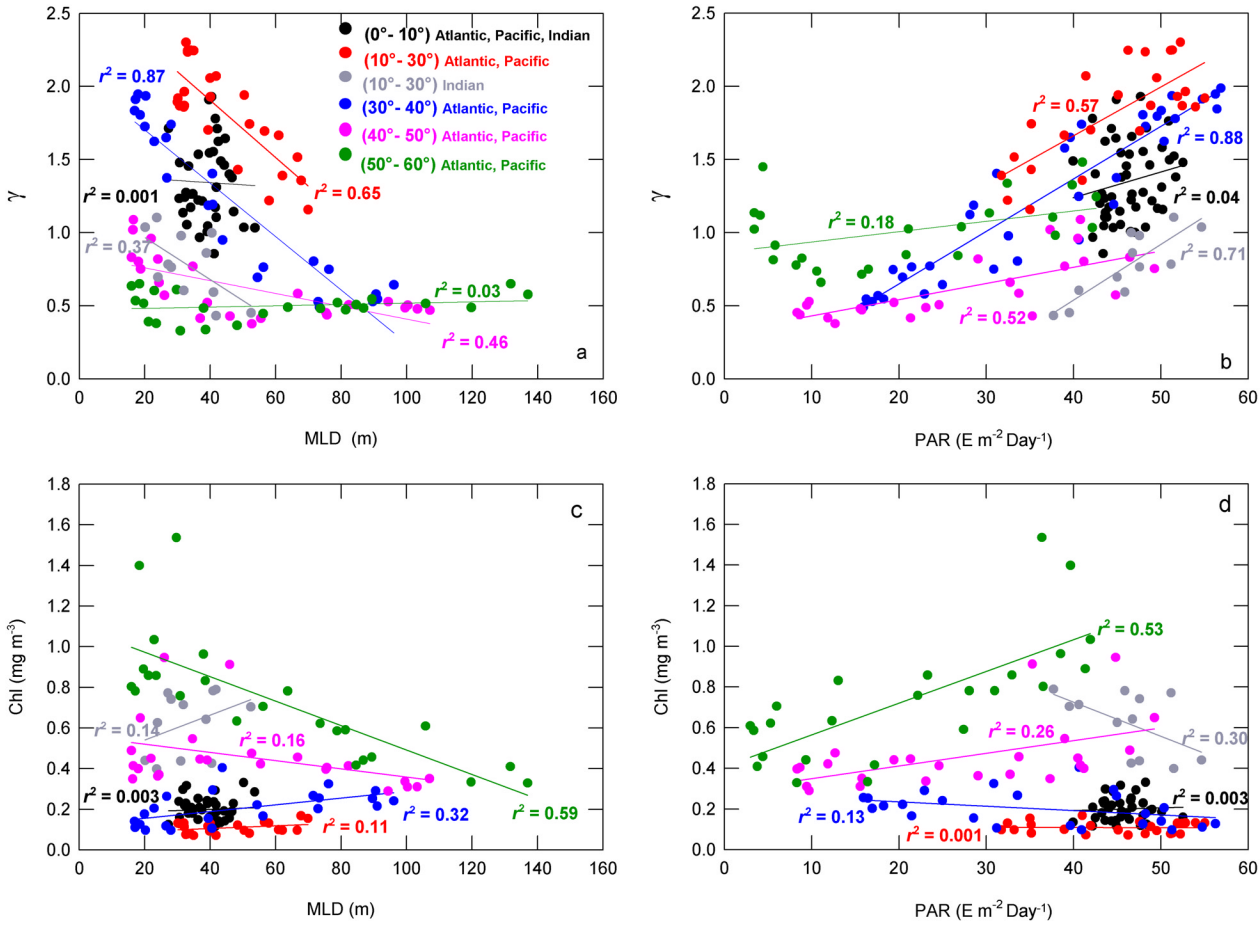

Figure 10. (a) Variation of monthly mean γ values in 2001 as a function of monthly mean MLD values for different latitudinal zones of the northern portion of the global ocean as indicated. (b) As in Figure 10a, but for γ and PAR. Solid lines represent the least squares linear regression fits performed on the different data sets. (c) Variation of monthly mean Chl values in 2001 as a function of monthly mean MLD values for different latitudinal zones of the northern portion of the global ocean as indicated. (d) As in Figure 10c, but for Chl and PAR.

[27] The different seasonal patterns of γ reported in this study for different oceanic regions are certainly affected by processes that modify the composition of particulate assemblages and physiology of phytoplankton in response to environmental forcing. This is supported by Figures 10a and 10b that show the variation of monthly values of γ as a function of MLD and PAR calculated for different latitudinal zones of the northern hemisphere (similar patterns are also observable in the southern hemisphere). Changes in γ are clearly related to variations in MLD and PAR for the [10°–30°N], [30°–40°N], and [40°–50°N] zones. Compared to the north tropical Atlantic and Pacific Oceans, the north tropical Indian Ocean presents much lower γ values but similar trends in γ vs. PAR and γ vs. MLD relationships (Figures 10a and 10b). The determination coefficient r^2 for the linear fits between γ and PAR is 0.88 and 0.52 for the [30°–40°N] and [40°–50°N] zones, respectively. For γ vs. MLD, the r^2 values are 0.87 and 0.46. When PAR increases and MLD shallows, γ tends to increase indicating a higher proportion of small particles compared to larger ones in stratified surface layers during summer season. Note that while similar responses of γ to the PAR and MLD variations are noticeable in the [10°–30°N] and [30°–40°N] zones, a much lower sensitivity to PAR and MLD is observed in the [40°–50°N] zone.

[28] For comparison, the variations in monthly values of Chl as a function of MLD and PAR calculated for the various latitudinal zones are shown in Figures 10c and 10d, respectively. Compared to γ, the changes in Chl show a much lower sensitivity to PAR and MLD, except in the [50°–60°N] zone. At these latitudes, the Chl concentration responds rapidly to the shoaling and deepening of the mixed layer depth. The generally poor relationships in Figures 10c and 10d can be attributed, at least partly, to differences in time scales or temporal shifts involved in phytoplankton responses and MLD changes between the minimum and maximum values, which control the availability of nutrients and light necessary for phytoplankton growth. As an example, these effects are particularly well seen in the [30°–40°] zone of the Atlantic and Pacific Oceans. We verified that in this zone the r^2 coefficient for the linear fit between Chl and MLD would increase from 0.32 to 0.73 if we correlated the

monthly Chl values with the monthly MLD values that are shifted one month back relative to Chl.

4. Conclusions

[29] We demonstrated the possibility of estimating the spectral dependency of particulate backscattering coefficient from satellite observations of ocean color. Unfortunately, in situ measurements of $b_{bp}(\lambda)$ are still very scarce, which does not allow to perform a rigorous validation of our estimation of γ. However, our γ values are consistent with previous estimation from inverse modeling and some recent field measurements. Moreover, the relationships we found between the satellite-derived γ and Chl are consistent with analogous relationships developed from in situ measurements. Future improvements of the satellite retrieval of γ are closely related to our ability to improve the retrieval of $K_d(\lambda)$ from space, and to the availability of additional spectral channels in the green and red parts of the spectrum to limit the effect of absorption.

[30] We found that the yearly value of γ ranges between 0 and 3.5 over the global ocean, with a mean value of 1.37 (standard deviation ±0.42). The spatial distribution of the monthly or annual mean values of γ is consistent with a prediction of a decrease of γ from oligotrophic to eutrophic regions, although significant regional differences in the γ vs. Chl relationship do exist. Seasonal variations of γ indicate that the proportion of small-sized particles compared to larger particles increases from winter to summer in the surface waters of the global ocean. The seasonal patterns of Chl, $b_{bp}(490)$, and γ exhibit differences in oceanic regions that are characterized by different physical forcing and biogeochemical conditions. These differences suggest that the dynamics of the particulate assemblage is closely related to the processes of growth and decline of phytoplankton population. The highest values of γ observed in the Pacific subtropical gyre are supported by recent field measurements of the high proportion of small-sized particles that accumulate in summer stratified layer in that region, as already suggested by *Dandonneau et al.* [2003].

[31] While our satellite-based estimation of γ opens new ways for advancing remote assessment of biogeochemical processes (such as the link between primary production and export), the interpretation of this capability in terms of particle size parameters does need further research. Numerous measurements performed in various oceanic regions suggested that the particle size distribution of living and nonliving suspended particles can be approximated by a power law or a Junge-type distribution [*Jonasz*, 1983; *Twardowski et al.*, 2001]. This approximation is often made with a single slope ξ, at least over some restricted range of particle size. The greater ξ (the steeper the slope), the more small particles relatively to large particles are present in water (and vice versa). Theoretical and experimental studies showed that the ξ value can be estimated from the spectral dependency of the particulate beam attenuation coefficient, c_p [*Morel*, 1976; *Boss et al.*, 2001]. Unfortunately, c_p appears to be difficult to estimate from satellite measurements because it is strongly governed by forward scattering, that is by scattered photons that do not leave the ocean. According to recent field measurements and theoretical studies [*Reynolds et al.*, 2001; *Morel and Maritorena*, 2001], the backscattering spectrum $b_{bp}(\lambda)$ can also provide approximate information on particle sizes. The γ values reported here are qualitatively interpreted as representing the relative proportion between small-sized and larger particles, so in that sense the γ values are related to the general slope ξ of the PSD. However, no quantitative relationships between γ and ξ have been developed yet. The difficulties arise from the lack of proper instrumentation and techniques for routine particle size determinations over the entire optically significant size range, including submicrometer particles. In addition, even if such measurements become available, there might be a conceptual difficulty to overcome because the simple parameterization of the real size distributions with a single slope over the entire size range seems to be inappropriate (see Figure 5). Nevertheless, because of potential implications of our study for research in ocean biogeochemistry, further efforts towards quantification of the relationships between the slope parameters γ and ξ and the uncertainties associated with such slope parameterizations are needed.

[32] **Acknowledgments.** This is a contribution of the BIOSOPE group (PROOF-JGOFS-France). This work was supported by Centre National d'Etude Spatiale in the frame of the TOSCA program. Partial support was also provided by NASA grant NNG04GO02G (awarded to D.S.). We thank E. Boss and D. Siegel for invaluable comments on the manuscript. In situ backscattering and chlorophyll (HPLC) measurements were obtained from the SeaBASS archive at the NASA Goddard Space Flight Center (GSFC). The Orbimage Corporation and the SeaWiFS Project at NASA/GSFC are acknowledged for providing the SeaWiFS ocean color data.

References

Aumont, O., E. Maier-Reimer, S. Blain, and P. Monfray (2003), An ecosystem model of the global ocean including Fe, Si, P co-limitations, *Global Biogeochem. Cycles*, *17*(2), 1060, doi:10.1029/2001GB001745.

Bader, H. (1970), The hyperbolic distribution of particle sizes, *J. Geophys. Res.*, *75*, 2822–2830.

Behrenfeld, M. J., E. Boss, D. A. Siegel, and D. M. Shea (2005), Carbon-based ocean productivity and phytoplankton physiology from space, *Global Biogeochem. Cycles*, *19*, GB1006, doi:10.1029/2004GB002299.

Boss, E., M. S. Twardowski, and S. Herring (2001), The shape of the particulate beam attenuation spectrum and its relation to the size distribution of oceanic particles, *Appl. Opt.*, *40*, 4885–4893.

Boss, E., W. S. Pegau, M. Lee, M. Twardowski, E. Shybanov, G. Korotaev, and F. Baratange (2004), Particulate backscattering ratio at LEO 15 and its use to study particle composition and distribution, *J. Geophys. Res.*, *109*, C01014, doi:10.1029/2002JC001514.

Bricaud, A., A. Morel, and L. Prieur (1983), Optical efficiency factors of some phytoplankters, *Limnol. Oceanogr.*, *28*, 816–832.

Brown, O. B., and H. R. Gordon (1974), Size-refractive index distribution of clear coastal water particulates from light scattering, *Appl. Opt.*, *13*, 2784–2822.

Carder, K. L., F. R. Chen, Z. P. Lee, S. Hawes, and D. Kamykowski (1999), Semi-analytic MODIS algorithms for chlorophyll a and absorption with bio-optical domains based on nitrate-depletion temperatures, *J. Geophys. Res.*, *104*, 5403–5421.

Ciotti, A. M., J. J. Cullen, and M. R. Lewis (1999), A semi-analytical model of the influence of phytoplankton community structure on the relationship between light attenuation and ocean color, *J. Geophys. Res.*, *104*, 1559–1578.

Claustre, H., and S. Maritorena (2003), The many shades of ocean blue, *Science*, *302*, 1514–1515.

Cota, G. F., W. G. Harrison, T. Platt, S. Sathyendranath, and V. Stuart (2003), Bio-optical properties of the Labrador Sea, *J. Geophys. Res.*, *108*(C7), 3228, doi:10.1029/2000JC000597.

Dandonneau, Y., A. Vega, H. Loisel, Y. du Penhoat, and C. Menkes (2003), Oceanic Rossby Waves acting as a "Hay Rake" for ecosystem floating by products, *Science*, 1548–1551.

De Boyer Montégut, C., G. Madec, A. S. Fischer, A. Lazar, and D. Iudicone (2004), Mixed layer depth over the global ocean: An examination of profile data and a profile-based climatology, *J. Geophys. Res.*, *109*, C12003, doi:10.1029/2004JC002378.

Dupouy, C., H. Loisel, J. Neveux, C. Moulin, S. Brown, J. Blanchot, A. Lebouteiller, and M. Landry (2003), Microbial absorption and backscattering coefficients from in situ and POLDER satellite during an El Nino-Southern Oscillation cold phase in the equatorial Pacific (180°), *J. Geophys. Res.*, *108*(C12), 8138, doi:10.1029/2001JC001298.

Falkowski, P. G., R. T. Barber, and V. Smetacek (1998), Biogeochemical controls and feedbacks on ocean primary production, *Science*, *281*, 200–206.

Frouin, R., B. A. Franz, and P. J. Werdell (2003), The SeaWiFS PAR product, *NASA Tech. Memo., 2003-206892*, *22*, 46–49.

Hoge, F. E., and P. E. Lyon (1996), Satellite retrieval of inherent optical properties by linear matrix inversion of oceanic radiance models: An analysis of model and radiance measurement errors, *J. Geophys. Res.*, *101*, 16,631–16,648.

Jonasz, M. (1983), Particles size distributions in the Baltic, *Tellus*, *35B*, 346–358.

Kitchen, J. C., and J. R. Zaneveld (1992), A three-layered sphere model of the optical properties of phytoplankton, *Limnol. Oceanogr.*, *37*, 1680–1690.

Koike, I., S. Hara, K. Terauchi, and K. Kogure (1990), Role of submicrometer particles in the ocean, *Nature*, *345*, 242–244.

Lal, D. (1977), The oceanic microcosm of particles, *Science*, *198*, 997–1009.

Loisel, H., and D. Stramski (2000), Estimation of the inherent optical properties of natural waters from irradiance attenuation coefficient and reflectance in the presence of Raman scattering, *Appl. Opt.*, *39*, 3001–3011.

Loisel, H., D. Stramski, B. G. Mitchell, F. Fell, V. Fournier-Sicre, B. Lemasle, and M. Babin (2001), Comparison of the ocean inherent optical properties obtained from measurements and inverse modeling, *Appl. Opt.*, *36*, 769–777.

Loisel, H., J. M. Nicolas, P. Y. Deschamps, and R. Frouin (2002), Seasonal and inter-annual variability of the particulate matter in the global ocean, *Geophys. Res. Lett.*, *29*(24), 2196, doi:10.1029/2002GL015948.

Longhurst, A. R., et al. (1992), Sub-micron particles in northwest Atlantic shelfwater, *Deep Sea Res.*, *39*, 1–7.

Melin, F., J.-F. Berthon, and G. Zibordi (2005), Assessment of apparent and inherent optical properties derived from SeaWiFS with field data, *Remote Sens. Environ.*, *97*, 540–553.

Morel, A. (1976), Diffusion de la lumière par les eaux de mer; résultats expérimentaux et approche théorique, *AGARD Lect. Ser.*, 3.1.1.–3.1.76.

Morel, A., and Y.-H. Ahn (1991), Optics of heterotrophic nanoflagellates and ciliates: A tentative assessment of their scattering role in oceanic waters compared to those of bacterial and algal cells, *J. Mar. Res.*, *49*, 177–202.

Morel, A., and S. Maritorena (2001), Bio-optical properties of oceanic waters: A reappraisal, *J. Geophys. Res.*, *106*, 7763–7780.

O'Reilly, J. E., et al. (2000), Ocean color chlorophyll a algorithms for SeaWiFS, OC2, and OC4: Version 4, in *SeaWiFS Postlaunch Technical Report Series*, vol. 11, *SeaWiFS Postlaunch Calibration and Validation Analyses, Part 3*, edited by S. B. Hooker and E. R. Firestone, pp. 9–23, NASA Goddard Space Flight Cent., Greenbelt, Md.

Reynolds, R. A., D. Stramski, and B. G. Mitchell (2001), A chlorophyll-dependent semianalytical reflectance model derived from field measurements of absorption and backscattering coefficients within the Southern Ocean, *J. Geophys. Res.*, *106*, 7125–7138.

Sathyendranath, S., L. Prieur, and A. Morel (1989), A three-component model of ocean colour and its application to remote sensing of phytoplankton pigments in coastal waters, *Int. J. Remote Sens.*, *10*, 1373–1394.

Sheldon, R. W., A. Prakash, and W. H. Sutcliffe (1972), The size distributions of particles in the ocean, *Limnol. Oceanogr.*, *17*, 327–340.

Smith, R. C. (1981), Remote sensing and depth distribution of ocean chlorophyll, *Mar. Ecol. Prog. Ser.*, *5*, 359–361.

Stramska, M., D. Stramski, R. Hapter, S. Kaczmarek, and J. Ston (2003), Bio-optical relationships and ocean color algorithms for the north polar region of the Atlantic, *J. Geophys. Res.*, *108*(C5), 3143, doi:10.1029/2001JC001195.

Stramski, D., and D. A. Kiefer (1991), Light scattering by microorganisms in the open ocean, *Prog. Oceanogr.*, *28*, 343–383.

Stramski, D., and J. Tegowski (2001), Effects of intermittent entrainment of air bubbles by breaking wind waves on ocean reflectance and underwater light field, *J. Geophys. Res.*, *106*(C12), 31,345–31,360.

Stramski, D., and S. B. Wozniak (2005), On the role of colloidal particles in light scattering in the ocean, *Limnol. Oceanogr.*, *50*, 1581–1591.

Stramski, D., A. Bricaud, and A. Morel (2001), Modeling the inherent optical properties of the ocean based on the detailed composition of planktonic community, *Appl. Opt.*, *40*, 2929–2945.

Stramski, D., E. Boss, D. Bogucki, and K. J. Voss (2004), The role of seawater constituents in light backscattering in the ocean, *Prog. Oceanogr.*, *61*, 27–56.

Terrill, E. J., W. K. Melville, and D. Stramski (2001), Bubble entrainment by breaking waves and their influence on optical scattering in the upper ocean, *J. Geophys. Res.*, *106*(C8), 16,815–16,823.

Toole, D. A., and D. A. Siegel (2001), Modes and mechanisms of ocean color variability in the Santa Barbara Channel, *J. Geophys. Res.*, *106*, 26,985–27,000.

Treguer, P., D. M. Nelson, A. J. Van Bennekom, D. J. Demaster, A. Leynaert, and B. Queguiner (1995), The balance of silica in the world ocean: A re-estimate, *Science*, *268*, 375–379.

Twardowski, M., E. Boss, J. B. Macdonald, W. S. Pegau, A. H. Barnard, and J. R. V. Zaneveld (2001), A model for estimating bulk refractive index from the optical backscattering ratio and the implications for understanding particle composition in case I and case II waters, *J. Geophys. Res.*, *106*, 14,129–14,142.

Werdell, P. J., and S. B. Bailey (2005), An improved bio-optical data set for ocean color algorithm development and satellite data product validation, *Remote Sens. Environ.*, *98*, 122–140.

Wozniak, S. B., and D. Stramski (2004), Modeling the optical properties of mineral particles suspended in seawater and their influence on ocean reflectance and chlorophyll estimation from remote sensing algorithms, *Appl. Opt.*, *43*, 3489–3503.

Yamasaki, A., H. Fukuda, R. Fukuda, T. Miyajima, T. Nagata, H. Ogawa, and I. Koike (1998), Submicrometer particles in northwest Pacific coastal environments: Abundance, size distribution, and biological origins, *Limnol. Oceanogr.*, *43*, 536–542.

Zhang, X., M. Lewis, M. Lee, B. Johnson, and G. Korotaev (2002), The volume scattering function of natural bubble populations, *Limnol. Oceanogr.*, *47*, 1273–1282.

H. Loisel and A. Poteau, ELICO - Université du Littoral - Côte d'Opale, F-62930 Wimereux, France. (loisel@mren2.univ-littoral.fr)

J.-M. Nicolas, Laboratoire d'Optique Atmosphérique, F-59655 Lille, France.

A. Sciandra, Laboratoire d'Océanologie de Villefranche-sur-Mer, F-06234 Villefranche-sur-Mer, France.

D. Stramski, Scripps Institution of Oceanography, University of California, San Diego, CA 92093-0238, USA.